Biomaterials Science

A noncanonical endocytic pathway is involved in the internalization of 3 μm polystyrene beads into HeLa cells

Journal:	*Biomaterials Science*
Manuscript ID	BM-ART-08-2022-001353.R1
Article Type:	Paper
Date Submitted by the Author:	19-Oct-2022
Complete List of Authors:	Hirose, Hisaaki; Kyoto University, Institute for Chemical Research Maekawa, Masashi; Keio University, Graduate School of Pharmaceutical Sciences Ida, Hiroki; Nagoya University, Graduate School of Engineering; Tohoku University, The Frontier Research Institute for Interdisciplinary Sciences; Japan Science and Technology Agency, Precursory Research for Embryonic Science and Technology Kuriyama, Masashi; Kyoto University, Institute for Chemical Research Takahashi, Yasufumi; Kanazawa Daigaku, Futaki, Shiroh; Kyoto University, Institute for Chemical Research

The manuscript for Biomaterials Science (RSC)
Paper (Regular Article)

A noncanonical endocytic pathway is involved in the internalization of 3 μm polystyrene beads into HeLa cells

Hisaaki Hirose[1]*, Masashi Maekawa[2], Hiroki Ida[3,4,5,6,7], Masashi Kuriyama[1], Yasufumi Takahashi[3,8], Shiroh Futaki[1]*

[1] Institute for Chemical Research, Kyoto University, Uji, Kyoto 611-0011, Japan
[2] Division of Physiological Chemistry and Metabolism, Graduate School of Pharmaceutical Sciences, Keio University, Minato-ku, Tokyo 105-8512, Japan
[3] Department of Electrical Engineering, Graduate School of Engineering, Nagoya University, Aichi 464-8601, Japan
[4] The Frontier Research Institute for Interdisciplinary Sciences, Tohoku University, Miyagi 980-8578, Japan
[5] Precursory Research for Embryonic Science and Technology, Science and Technology Agency (JST), Saitama 332-0012, Japan
[6] Advanced Institute for Materials Research, Tohoku University, Miyagi 980-8577, Japan
[7] Graduate School of Environmental Studies, Tohoku University, Miyagi 980-8579, Japan
[8] WPI Nano Life Science Institute (WPI NanoLSI), Kanazawa University, Ishikawa 920-1192, Japan

*Corresponding: hirose.hisaaki.5m@kyoto-u.ac.jp, futaki@scl.kyoto-u.ac.jp

Abstract

Extracellular fine particles of various sizes and origins can be taken up by cells, affecting their function. Understanding the cellular uptake processes is crucial for understanding the cellular effects of these particles and the development of means to control their internalization. Although macropinocytosis is a possible pathway for the cellular uptake of particles larger than 0.2 μm, its contribution to cellular uptake in non-phagocytotic cells is controversial. Using 3 μm polystyrene beads as a model particle, we aimed to assess the detailed modes of their cellular uptake by non-phagocytic HeLa cells. Cellular uptake was assessed using confocal, scanning electron, and scanning ion conductance microscopy analyses, together with inhibitor studies. Our results revealed that 3 μm beads were taken up by HeLa cells by an actin-, cholesterol-, and membrane protrusions-dependent noncanonical endocytotic pathway, different from the canonical macropinocytotic and phagocytotic pathways. Our work provides a framework for studying the cellular uptake of extracellular fine particles.

Keywords: polystyrene beads, endocytosis, phagocytosis, macropinocytosis, cholesterol

1. Introduction

Cells can take up extracellular fine particles of various sizes ranging from nanometers to micrometers.[1-3] These fine particles can influence the function of the cells and include exogenous fine particles, such as polymer-/lipid-based nanomaterials, microplastics, and PM2.5, and endogenous fine particles of *in vivo* origins, such as extracellular vesicles, including microvesicles and exosomes. Understanding the modes of cellular uptake and the intracellular fates of these particles is highly important to elucidate and control the biological responses caused by extracellular fine particles. For the cellular uptake of extracellular fine particles in sub-micrometer to micrometer size ranges, two forms of endocytosis, *i.e.*, phagocytosis and macropinocytosis, can be the predominant pathways; in other representative forms of endocytosis, such as clathrin-mediated endocytosis and caveolae-mediated endocytosis, the sizes of the vesicles are generally < 0.2 μm in diameters,[4] which are too small to accommodate these extracellular particles.

Phagocytosis is a special form of endocytosis by which cells engulf and uptake large extracellular particles, including microbial pathogens, by closely adhering to the plasma membrane and excluding the extracellular fluids surrounding the particles.[5, 6] Phagocytosis is observed in only specialized cells termed phagocytes including macrophages, neutrophils, monocytes, dendritic cells, and osteoclasts.[5] In contrast,

macropinocytosis is a non-selective actin-dependent cellular uptake that allows cells to engulf a large volume of fluids, solutes, and nutrients.[7] Macropinocytosis is categorized as stimuli-driven endocytosis; although it is constitutively active in phagocytic cells and certain types of cancer cells, it does not occur in non-phagocytic cells without specific stimuli such as growth factors. The sizes of macropinosomes, which are formed by macropinocytosis, range from 0.2-10 μm in diameters.[5] Thus, macropinocytosis has been considered a potential major route for cellular uptake of extracellular fine particles by non-phagocytic cells.

Polystyrene particles/beads have been employed as models to study the cellular uptake processes of extracellular fine particles because their functions and sizes can be easily manipulated.[1] A previous study has reported the lack of internalization of 1-3 μm-sized polystyrene beads into non-phagocytic HeLa cells without surface coating using transfection agents.[8] In contrast, several studies have reported the internalization of polystyrene beads into non-phagocytic cells. For example, Zauner et al. have reported the cellular uptake of polystyrene beads (up to 1 μm) by non-phagocytic cell lines (HUVEC, ECV-304, and HNX-14C). [9] Similarly, Rejman et al. have reported the cellular uptake of polystyrene beads (up to 0.5 μm) by B16 melanoma cells.[10] However, the contribution of macropinocytosis to the cellular uptake of polystyrene beads by these non-phagocytic

cells remains controversial. Several previous analyses on the cellular uptake of extracellular fine particles were predominantly based on sensitivity to inhibitors of endocytosis. However, inhibitors of endocytosis often have multiple effects on cellular processes, and sensitivity to these inhibitors differs depending on the cell type and incubation conditions. Therefore, the results of studies using these inhibitors often have room for debate and further analysis.[11]

This study aimed to comprehensively investigate whether 3 μm polystyrene beads are effectively taken up by non-phagocytic HeLa cells and whether the canonical characteristics of macropincytosis are accompanied by this step, using inhibitors and morphological studies through the analyses of live cell confocal laser scanning microscopy (CLSM), scanning electron microscopy (SEM) and scanning ion conductance microscopy (SICM). Moreover, owing to the size of the 3 μm polystyrene beads, we observed the interplay between the beads and cells in real-time using CLSM and SICM. Labeling the beads with a pH-sensitive dye, pHrodo, allowed us to identify and quantify endosome-trapped beads taken up into the cells.

In this study, we found that 3 μm polystyrene beads are internalized into HeLa cells in a serum-containing medium in 24 h, even without a transfection reagent. Notably, the 3 μm beads are efficiently endocytosed into the cells within 2 h when incubated in

serum-free condition, which is unlikely to evoke macropinocyotosis in HeLa cells due to the absence of stimuli such as chemokines.[12] Our results indicated that the 3 μm polystyrene beads are internalized into HeLa cells by a noncanonical actin-driven endocytosis pathway, which may be different from conventional macropinocytosis and phagocytosis.

2. Experimental Section

2.1 Materials

Polybead amino and carboxylate microspheres (3 μm) were purchased from Polysciences (Warrington, PA, USA). The pHrodo Red succinimidyl ester, the pHrodo Green STP ester, Tetramethylrhodamine (TMR)-dextran (10 kDa), and bovine serum (BS) were purchased from Thermo Fisher Scientific (Waltham, MA, USA). Chlorpromazine (CPZ), 5-(*N*-ethyl-*N*-isopropyl)amiloride (EIPA), nystatin, and LY294002 were purchased from Sigma-Aldrich (St. Louis, MO, USA). Latrunculin A (LatA) and methyl-β-cyclodextrin (MβCD) were purchased from Fujifilm Wako (Osaka, Japan). Alexa Fluor 488 anti-human CD147 and Alexa Fluor 647 anti-human CD71 antibodies were purchased from BioLegend (San Diego, CA, USA). HMRef, an F-actin staining reagent, was a kind gift from Prof. Y. Urano (The University of Tokyo, Japan).[13] Other reagents, including salts

and culture media, were obtained from Sigma-Aldrich and Fujifilm Wako unless otherwise specified.

2.2 pHrodo labeling

pHrodo labeling on the amino beads (3 μm) was performed using the pHrodo Red succinimidyl ester or the pHrodo Green STP ester as previously described.[8] Briefly, amino beads were washed, resuspended in 100 mM sodium hydrogen carbonate (pH 8.4), and reacted with pHrodo ester for 1 h at 25 °C. The beads were washed with PBS three times and then resuspended in PBS.

2.3 Cell culture

HeLa cells (human epithelial carcinoma cell line) and U2OS cells (human osteosarcoma cell line) were obtained from the European Collection of Authenticated Cell Cultures (ECACC). hTERT-RPE1 cells (immortalized human retinal pigment epithelial cell line) were obtained from American Type Culture Collection (ATCC). HeLa cells were cultured in α-minimum essential medium (α-MEM) supplemented with 10% (v/v) heat-inactivated bovine serum (BS) (referred to as α-MEM(+)). U2OS cells were cultured in high glucose Dulbecco's modified eagle medium (DMEM) supplemented with 10% (v/v)

heat-inactivated fetal bovine serum (FBS). RPE1 cells were cultured in DMEM/Ham's F-12 (DMEM/F12) supplemented with 10% (v/v) heat-inactivated FBS. The cells were maintained at 37 °C in a humidified 5% CO_2 incubator.

2.4 Confocal microscopy

HeLa cells were seeded onto 35 mm glass-bottom dishes (Iwaki, Shizuoka, Japan) and were allowed to reach 70-80% confluence in 24 h. The cells were washed with PBS and then incubated with pHrodo-beads (100 μg/mL) in α-MEM(+), α-MEM(–) (or isotonic buffer), hypotonic buffer (0.5× α-MEM(–)), or hypertonic buffer (α-MEM(–) containing 0.2 M sucrose) at 37 °C for 2 or 24 h. Then α-MEM(+) was added and observed using an FV3000 CLSM system (Olympus, Tokyo, Japan) equipped with a 60× oil immersion objective lens (UPlanSApo, NA 1.35; Olympus). For treatment with inhibitors, the cells were pretreated with DMSO (vehicle), CPZ (5 μg/mL), EIPA (25 μM), nystatin (50 μM), MβCD (10 mM), LY294002 (10 μM), or LatA (0.2 μM) in α-MEM(–) for 30 min. Then the cells were then washed with PBS and incubated with pHrodo-beads (100 μg/mL) in α-MEM(–) for 2 h in the presence of inhibitors, except for MβCD and LatA. MβCD and LatA were only pretreated to avoid cytotoxicity. The number of pHrodo-beads in each cell was analyzed and quantified using Fiji/ImageJ (ver. 2.3.0/1.53q) based on increased

pHrodo fluorescence intensities.

For CD147 and CD71 staining, the cells were incubated with Alexa Fluor 488-labeled anti-human CD147 antibody (1:100) and Alexa Fluor 647-labeled anti-human CD71 antibody (1:100) in α-MEM(–), respectively, for 45 min at 37 °C in a humidified 5% CO_2 incubator. For F-actin staining, the cells were incubated with HMRef (1 μM) in α-MEM(–) for 30 min at 37 °C in a humidified 5% CO_2 incubator. For time-lapse imaging, the cells were washed three times with α-MEM(–) or PBS, and then incubated in 150 μL of α-MEM(–) in an STX stage top incubator (TOKAI HIT, Shizuoka, Japan), humidified with 5% CO_2 at 37 °C, attached to FV3000 CLSM system. To observe the TMR-dextran fluid-phase uptake, the cells were incubated in α-MEM(–) containing TMR-dextran (0.5 mg/mL). Time-lapse images were acquired every 30 sec or 2 min, and the pHrodo-beads (50 μL; final concentration of 100 μg/mL) were added to the medium 5 or 10 min after time-lapse imaging was started. Images were analyzed using the Fiji/ImageJ software.

2.5 Scanning electron microscopy

HeLa cells were seeded onto 35 mm glass-bottom dishes (Iwaki) and were allowed to reach 70-80% confluence in 24 h. The cells were washed with PBS and pretreated with

DMSO (vehicle) or 10 mM of MβCD in α-MEM(–) for 30 min. The cells were then washed with PBS and incubated with pHrodo-beads (100 μg/mL) in α-MEM(–) at 37 °C for 30 min. The cells were washed with pre-warmed (30-35 °C) 0.1 M cacodylate buffer (pH 7.4) and then fixed with 2% glutaraldehyde and 4% paraformaldehyde in 0.1 M cacodylate buffer (pH 7.4) for 1 h at 25 °C. The cells were washed with cacodylate buffer, and post-fixed with 1% osmium tetroxide in cacodylate buffer for 2 h. The samples were washed with distilled water and then subjected to the conductive staining with 1% buffered osmium tetroxide and 1% tannic acid (O-T-O methods). The samples were dehydrated using a graded series of ethanol and critical-point drying methods (Critical Point Dryer HCP-1; Hitachi, Ltd., Tokyo, Japan), coated with a thin layer (3 nm) of osmium coater (HPC-30W; Vacuum Device Inc., Ibaraki, Japan), and then observed with a field-emission scanning electron microscope (Hitachi S-4800,) at an acceleration voltage of 2 kV.

2.6 Time-lapse imaging using scanning ion conductance microscopy

The SICM setup has been described in previous reports.[14] A nanopipette (inner diameter: approximately 100 nm), which was used as a probe, was filled with Leibovitz's L-15 medium (Gibco, Thermo Fisher Scientific) without serum [L-15 (–)).[15] The nanopipette

was also inserted into an Ag/AgCl electrode. Before the measurements, HeLa cells seeded onto a 35 mm glass-based dish (Iwaki) were washed twice with L-15(–) and added in L-15(–). The dish was set on the XY-piezo stage of the SICM setup. The nanopipette and an Ag/AgCl electrode were immersed in L-15(–) in the dish. The position of the nanopipette was aligned near the cell using optical microscopy, and a decrease in the ion current was used as a feedback signal. Before time-lapse imaging using SICM, the 3 μm pHrodo-beads were added, and then pipetted up and down. The elapsed time was calculated after the sample was pipetted. The time-lapse images were obtained at 8 × 8 μm^2 with 64 × 64 pixels. One scanning in the time-lapse images was completed in approximately 2 min.

2.7 Statistical analysis

All data for the quantification of internalized beads are shown as dot plots with the mean ± standard error of the mean (S.E.M) of three independent experiments. All statistical analyses were performed using the GraphPad Prism (version 9.4.0). The Mann-Whitney test and Kruskal-Wallis tests were used to compare two groups and multiple groups, respectively. Statistical significance was set as $P < 0.05$.

Results and Discussion

Cellular uptake of pHrodo-labeled 3 μm polystyrene beads is dependent on cholesterol and actin dynamics

To assess the cellular uptake of 3 μm polystyrene beads, we labeled polystyrene amino beads with pHrodo (pHrodo-beads) according to a previous report.[8] As pHrodo is a pH-sensitive dye whose fluorescence is increased with endosomal acidification,[16] pHrodo-beads in endosomes can be differentiated from those outside the cells by fluorescence microscopy, allowing us to follow their real-time localization and to quantify the number of pHrodo-beads inside cells. The pKa of pHrodo is approximately 6.5,[17] and the pH in the early endosomes is usually approximately 6.3.[18] Thus, the fluorescence intensity of pHrodo should increase significantly when the endocytic vesicles become early endosomes.

First, we examined whether the 3 μm beads were internalized into HeLa cells without transfection reagents in the presence or absence of serum. The cells were incubated with the pHrodo-labeled 3 μm beads in a serum-containing medium. Under this condition, we did not observe a substantial pHrodo signals in the cells at 2 h as previously reported.[8] However, we observed significant pHrodo signals in the cells after a longer incubation time (24 h) (**Fig. 1A;** 2 and 24 h in α-MEM(+)). Quantification of fluorescent

beads in more than 250 cells suggested that a few beads were taken up per cell after 24 h (**Fig. 1B;** 24 h in α-MEM(+)), although no substantive uptake was observed after 2 h of incubation in a serum-containing medium (**Fig. 1B;** 2 h in α-MEM(+)). Notably, the beads were considerably more efficiently internalized into HeLa cells in a serum-free medium after 2 h (**Fig. 1A;** 2 h in α-MEM(–)), with approximately 8 beads up-taken per cell (**Fig. 1B;** 2 h in α-MEM(–)). These results indicate that the fluorescent beads were captured in the acidic compartment of cells, suggesting the involvement of endocytosis in the internalization of the pHrodo-beads. In addition, internalization of the pHrodo-beads in other non-phagocytic cells, such as cancerous U2OS cells and non-cancerous RPE1 cells, was similarly traceable using this approach (**Supplementary Fig. S1**), where cellular localization of pHrodo-beads can be monitored through differential interference contrast (DIC) imaging and that in acidic endosomes can be discriminated with the fluorescent signals, suggesting the validity of analyzing the modes of cellular uptake using live cells.

To elucidate which modes of endocytosis are involved in the internalization of the pHrodo-beads, inhibitors of endocytosis, chlorpromazine (CPZ), 5-(*N*-ethyl-*N*-isopropyl)amiloride (EIPA), and nystatin were used to inhibit clathrin-mediated endocytosis, macropinocytosis, and caveolae-mediated endocytosis, respectively. Our

results showed that CPZ and EIPA did not significantly inhibit the cellular uptake of the pHrodo-beads (**Fig. 1C**). This suggests that clathrin-mediated endocytosis and macropinocytosis may not be involved in the internalization of the pHrodo-beads. In contrast, nystatin significantly inhibited the cellular uptake of the pHrodo-beads (**Fig. 1C**). In general, caveolae-mediated vesicles are approximately 60-80 nm in diameter;[19] therefore, it seems unlikely that the 3 μm beads are taken up by caveolae-mediated endocytosis. Other classical endocytic pathways that may be sensitive to cholesterol depletion, such as clathrin-independent carrier/glycosylphosphatidylinositol-anchored protein enriched early endocytic compartment (CLIC/GEEC) and fast endophilin-mediated endocytosis (FEME) pathways, also form endocytic vesicles at 60-100 nm diameter.[20] Thus, it is also unlikely that the 3 μm beads are taken up by these endocytic pathways. We instead suspected that the inhibitory effect observed in nystatin-treated cells may be due to cholesterol sequestration.[21] To examine the effect of cholesterol in the plasma membrane on cellular uptake of the pHrodo-beads, we used methyl-β-cyclodextrin (MβCD) to deplete cholesterol from the plasma membrane. MβCD significantly inhibited the cellular uptake of the pHrodo-beads (**Fig. 1D**), suggesting that the cellular uptake pathway of the pHrodo-beads is dependent on cholesterol in the plasma membrane.

Macropinocytosis and phagocytosis are highly dependent on actin, cholesterol, and phosphoinositide 3-kinase (PI3K).[22] Although HeLa cells are non-phagocytic cells, we investigated whether the cellular uptake process of the beads is similar to phagocytosis. We examined the effects of LY294002, a PI3K inhibitor, and Latrunculin A (LatA), an actin polymerization inhibitor, on cellular uptake of the pHrodo-beads (**Fig. 1E**). The cellular uptake of the beads was slightly, but significantly, inhibited by LY294002, whereas it was effectively inhibited by LatA. This suggests that the internalization of the pHrodo-beads is partly PI3K-dependent and strongly actin-dependent.

Furthermore, we examined the effects of changes in the membrane tension on cellular uptake. A previous study has reported that an increase in membrane tension is related to the phagocytotic process, and the internalization of particles taken up by phagocytosis is enhanced in a hypotonic buffer.[23] In contrast, another study has reported that macropinocytosis is induced by a decrease in membrane tension when using a hypertonic buffer.[24] Therefore, we compared the number of the internalized beads in the isotonic, hypotonic, or hypertonic buffers. The internalization of the beads was enhanced in the hypotonic buffer, whereas it was significantly inhibited in the hypertonic buffer (**Fig. 1F**). This suggests that cellular uptake of the beads may be affected by membrane tension and that the mode may be more similarity to phagocytosis than macropinocytosis.

Collectively, our quantification analyses suggested that the internalization of 3 μm pHrodo-labeled polystyrene beads into HeLa cells is highly dependent on cholesterol in the plasma membrane as well as actin dynamics, and is more similar to phagocytosis than macropinocytosis.

The internalization pathway of pHrodo-beads is unlikely to be canonical endocytosis or macropinocytosis

Although HeLa cells are not phagocytic cells, we cannot exclude the possibility of the involvement of phagocytosis or its related pathways in the cellular uptake of the pHrodo-beads. Therefore, we analyzed cellular uptake processes in live cells using time-lapse imaging. To confirm whether the endosomes encapsulating pHrodo-beads are clathrin-independent pathway, we investigated the internalization of the beads with cargo proteins of clathrin-dependent and -independent endocytoses, CD71 (also known as transferrin receptor) and CD147 (or Basigin, also known as an extracellular matrix metalloproteinase inducer, EMMPRIN), respectively.[25, 26] Following the procedure reported previously,[26] Alexa-labeled antibodies against these molecules were employed as markers to visualize the respective pathways.

HeLa cells were incubated with Alexa-labeled antibodies against CD147 and

CD71 to stain the proteins (**Fig. 2**). The arrowhead at 26 min in the DIC image shows a bead being taken up by the cell. No significant pHrodo-bead signal was observed at this time point, suggesting that the pH in the endosomes was not sufficiently acidic just after endosomal encapsulation of the bead. A CD147 (Alexa488) fluorescent signal with a round structure was also observed, suggesting that CD147 was taken up into endosomes together with the pHrodo-bead and that the endosomal membranes were closely located to the pHrodo-bead without a large volume of extracellular fluid. In contrast, no endosome-like signals at the corresponding position were observed with CD71 (Alexa647) immunofluorescent imaging. These results suggested the endocytic uptake of pHrodo-beads by clathrin-independent endocytosis, consistent with the above results using inhibitors of endocytosis (**Fig. 1C-F**). Notably, the simultaneous observation of internalizing beads using DIC and fluorescence imaging is an important advantage of using 3 μm pHrodo-beads. These results also suggest that the pHrodo-beads are enclosed by the cellular membrane without disrupting the endosomal membrane under the given conditions.

The pHrodo signal became notable at 44 min, likely because of acidification of the endosomes (**Fig. 2;** arrow). At this time point, the CD71 signal at the corresponding location of the bead became apparent, whereas the CD147 signal became less apparent.

These results suggest that the endosomes with CD71 signals were fused to the endosome encapsulating the pHrodo-beads and that endosomes containing the beads maturated by fusing late endosomes or lysosomes. Overall, our observations indicate that pHrodo-beads did not directly penetrate the cells but were instead endocytosed by a clathrin-independent pathway and trafficked, accompanied by endosomal acidification.

The beads used in this study were functionalized with amine groups. Since the cell surface is thought to be negatively charged, the positively charged surface of the particles may affect the cellular uptake of the beads. Labeling with fluorescence dye may lead to increase the hydrophobicity of the beads and thus affect the cellular uptake. To evaluate these effects, we examined cellular uptake of the amino-functionalized beads in comparison with carboxy-functionalized beads (3 μm) in the absence of pHrodo-labeling. Significant internalization of carboxy-functionalized beads was observed, however, with lesser efficacy than in the case of the amino-functionalized beads (**Supplementary Fig. S2**). No substantive effect of pHrodo-labeling on the cellular uptake of pHrodo-beads (amino-functionalized beads) was observed (Fig. 2 versus Supplementary Fig. S2A). These results suggested that the amino functionalization had an effect but that the amino groups were not indispensable for the cellular uptake of 3 μm beads.

We next examined whether actin accumulates with the uptake of beads, which is an important feature of both phagocytosis and macropinocytosis. To observe the

possible reorganization of actin filaments when the pHrodo-beads were internalized into live cells, we stained F-actin of HeLa cells with a cell-permeable small molecular weight compound HMRef (**Fig. 3**).[13] We then performed time-lapse imaging every 30 s after the cells were incubated with the pHrodo-beads. **Fig. 3A** shows 52.5 min after the addition of the pHrodo-beads. The arrow indicates one of the representative pHrodo-beads whose fluorescence started to increase (i.e., the early stage of endosomal acidification). **Fig. 3B** shows an inventory of time-lapse images of the area encircled in a yellow square in Fig. 3A. We observed that the actin filament was initially attached to the bead and endosome containing pHrodo-beads (**Fig. 3B;** arrowheads at 20 and 21.5 min). However, the actin structure surrounding the beads became obscure after the pHrodo-bead internalization was completed (**Fig. 3B;** at 37.5 min), followed by an increase in pHrodo fluorescence (**Fig. 3B;** the arrow at 52.5 min). However, this actin filament accumulation is less evident than that typically observed in the formation of phagosomes and macropinosomes.[27, 28]

As suggested from Fig. 2, endosomes encapsulating pHrodo-beads may not be accompanied by a large volume of extracellular fluids. We additionally examined the absence of non-selective fluid phase uptake accompanied by the bead internalization. Phagocytosis generally excludes fluid-phase when the cells take up particles because the plasma membrane closely attaches to the particles to form a phagosomal cup,[5, 6] whereas

macropinocytosis is associated with non-selective fluid-phase uptake.[29] To examine whether the internalization of the pHrodo-beads accompanies fluid-phase uptake, we used pHrodo Green-labeled beads and 10 kDa of tetramethylrhodamine (TMR)-dextran (TMR-dex10) as a fluid-phase marker (**Fig. 4**). In general, 70 kDa of dextran is used as a macropinocytosis marker;[30] however, we used a smaller size of dextran (10 kDa) to investigate whether a considerably small volume of the fluid-phase is taken up or excluded when the beads are internalized. We found that no substantial TMR-dex10 signals were accompanied by the internalization of the pHrodo-beads, which suggests that fluid-phase uptake was almost excluded and that the plasma membrane was closely attached to the beads to be taken up (**Fig. 4**). This result also suggests that the internalization of the pHrodo-beads seems to share more characteristics with phagocytosis than macropinocytosis.

Membrane protrusions on the cell surface are crucial for the internalization of the pHrodo-beads

Next, we performed SEM imaging to analyze changes in the cell surface when the cells were incubated with the pHrodo-beads (**Fig. 5**). As shown in Fig. 1, the pHrodo-beads internalization was highly dependent on cholesterol; therefore, we observed the cells 30

min after the incubation with the pHrodo-beads using MβCD. In the absence of the pHrodo-beads and MβCD, the cells were covered with slender membrane protrusions (**Fig. 5A;** control, magenta arrows). In contrast, MβCD treatment resulted in the shortening of membrane protrusions on the cell surface (**Fig. 5A;** MβCD, blue arrows). When the cells were incubated with the pHrodo-beads in the absence of MβCD treatment, the beads accumulated on the cell surface (**Fig. 5B;** control), with some beads being taken up into the cells (**Fig. 5B;** control, arrows**)**. A more detailed analysis of the boxed area in Fig. 5B-control revealed that the pHrodo-beads accumulated on the cell surface are captured by membrane protrusions and/or ruffle-like membranes (**Fig. 5 C;** control). Multiple numbers of membrane protrusions were attached to the pHrodo-beads to capture them (**Fig. 5C;** control, white arrowheads). In some cells, we also observed ruffle-like membranes close to the pHrodo-beads (**Fig. 5C;** control, yellow arrowheads). SEM observation revealed that the cellular uptake of the pHrodo-beads is likely different from typical phagocytosis which is accompanied by close adhesion of the plasma membrane to the particles. The pHrodo-beads were captured by membrane protrusions; however, canonical phagocytotic membrane structures were not observed to engulf the beads. Moreover, the close contact of membrane protrusions with pHrodo-beads indicates that macropinocytosis unlikely contribute to the cellular uptake of the beads.

As described above, MβCD treatment significantly affected the membrane protrusions structure on the cell surfaces (**Fig. 5A;** MβCD). Although there were similar numbers of pHrodo-beads attached to cell surfaces (**Fig. 5B;** MβCD), few beads were captured by the membrane protrusions (**Fig. 5 C;** MβCD). Moreover, consistent with Fig. 1D, no significant pHrodo-beads internalization was observed (**Fig. 5B and C;** MβCD), as indicated by Fig. 5B-control (white arrows). These results suggest that membrane protrusions are important for the internalization of the pHrodo-beads.

Membrane protrusions play a key role in the cellular uptake of the pHrodo-beads

To gain more insights into the relationship between the membrane protrusions dynamics and the pHrodo-beads uptake, we performed real-time and live cell observation of the cellular uptake of the beads using SICM imaging (**Fig. 6, and Supplementary Video S1**). SICM is a cutting-edge microscopy method using a glass nanopipette as an imaging probe to noninvasively obtain three-dimensional (3D) images of live cell surfaces at ≤100 nm resolution, allowing the observation of the dynamics of membrane protrusions on cell surface. We have previously exemplified the usefulness of SICM in the analysis of the plasma membrane dynamics by the interaction with an arginine-rich cell-penetrating peptide.[14] In the present study, SICM analysis suggested that upon their addition to cells,

the pHrodo-beads were captured by multiple numbers of membrane protrusions attaching on and detaching from the bead surface (**Fig. 6A;** white arrows at t = 03:20). The action of the membrane protrusions became less intense within a few to several minutes; however, some membrane protrusions likely remained attached to the beads (**Fig. 6A;** white arrows, images up to t = 22:23 are given). Prolonged observation of the bead in Fig. 6A showed that the bead remained attached to the cells surface until ~65 min (**Fig. 6B;** the upper bead with magenta arrowheads), and then it seems likely that the bead was suddenly internalized, without accompanied by marked morphological alterations of the cell membranes (**Fig. 6B;** green arrowhead, t = 70:03), which was completed in ~5 min. A similar mode of internalization was also observed for another bead in the image (Fig. 6B; the lower bead with yellow arrowheads). After repeated attachment of the membrane protrusions (**Fig. 6B;** white arrows), the bead appeared to suddenly being taken up into the cells (see **Fig. 6B**; green arrowhead, t = 48:07). No marked ruffle-like membrane structures were observed during the uptake process.

Notably, not all beads were internalized within 2 h, even when captured by the membrane protrusions. During our observation, SICM showed no obvious ruffle-like membrane structures when the beads were internalized into the cells, suggesting that the pHrodo-beads are internalized into the cells in a membrane protrusion-dependent manner.

Further studies are required to reveal the mechanism by which the capture of the beads by the membrane protrusions lead to their sudden internalization. Nonetheless, our findings suggest a novel internalization pathway of the beads, which is different from canonical macropinocytosis and phagocytosis.

Conclusion

In summary, we found that the internalization of 3 μm pHrodo-beads into non-phagocytic HeLa cells was highly dependent on cholesterol and actin. The central motivation of this study is to identify and characterize the unique cellular uptake modes of 3 μm beads by non-phagocytic HeLa cells. Using this bead size as well as CLSM, EM, and SICM observation, this study traced the uptake of the beads at the single particle level, allowing for the dissection of cellular events accompanied by the bead uptake. Such an approach may not be possible through conventional methods dealing with multiple molecules or events and thus yielding the sums and averages. Our study revealed that the cellular uptake pathway of the beads was not macropinocytosis, which has been conventionally assumed to be the main cellular uptake pathway of extracellular fine particles (> 0.2 μm) into non-phagocytic cells. We showed that the pHrodo-beads are internalized into non-phagocytic HeLa cells via a noncanonical endocytic pathway involving membrane protrusions. It would also be interesting to

examine whether there are differences in internalization modes of the beads among other non-phagocytic cell lines and phagocytic cells using this approach. Our work provides a novel framework for studying the cellular uptake of extracellular fine particles. This study also highlighted the importance of analyzing cellular uptake pathways using multiple analytical methods; novel and non-typical modes of cellular uptake can be overlooked via superficial analysis using only inhibitors. Investigations using cutting-edge technologies with considering the biological definitions of various endocytic pathways will reveal authentic cellular uptake pathways of extracellular particles of interest or discover uncanonical cellular uptake processes, resulting in improved development of particles for efficient drug delivery in the future.

Author Contribution

H.H. directed the project, performed experiments, analyzed data, and wrote the manuscript. M.M. advised about cell biological experiments and analyzed data. H.I. and Y.T. performed scanning ion conductance microscopy observation and analyzed data. M.K. performed experiments with H.H. S.F. supervised the project and wrote the manuscript with H.H.

Conflicts of interest

There are no conflicts to declare.

Acknowledgments

We thank Masachika Shudou at the Division of Medical Research Support, the Advanced Research Support Center (ADRES), Ehime University for his technical assistance of scanning electron microscopy. This work was supported by JSPS KAKENHI Grant Numbers JP20K22705 and JP22K05313 to H.H., and JST CREST (Grant Number JPMJCR18H5) to S.F. This work was supported by the International Collaborative Research Program of Institute for Chemical Research, Kyoto University (grant # 2021-112 to M.M.).

Figure legends

Fig. 1. Observation and quantification of pHrodo-beads (3 μm) internalized into HeLa cells. (A) Confocal microscopy observation of HeLa cells incubated with pHrodo-beads for 2 or 24 h in α-MEM(+) or 2 h in α-MEM(−). Scale bar, 50 μm. (B) Quantification of (A). The X-axis indicates the number of the internalized pHrodo-beads per cell. (C-F) Quantification of the number of the internalized pHrodo-beads per cell under each condition. Each dot represents the number of the internalized beads in a cell. Left to right: (B) n = 257, 257, and 266 cells; (C) n = 256, 258, 238, and 233 cells; (D) n = 252 and 251 cells; (E) n = 221, 232, and 227 cells; (F) n = 246, 257, and 234 cells, pooled from three independent experiments. Red bars represent the mean ± S.E.M. ****, $P < 0.0001$; ns, not significant. (B, C, E, F) Kruskal-Wallis test; (D) Mann-Whitney test. DIC, differential interference contrast.

Fig. 2. Time-lapse imaging of the internalization of pHrodo-beads into HeLa cells stained with Alexa-labeled antibodies against CD147 and CD71. HeLa cells were stained with Alexa-labeled antibodies against CD147 and CD71. Arrowheads indicate the early stage of internalization of pHrodo-beads; arrows indicate maturation or acidification of endosomes containing pHrodo-beads. Cyan color represents CD147 signal

(Alexa488); Magenta color represents pHrodo-bead signal; Yellow color represents CD71 signal (Alexa647). Scale bar, 20 μm. The time point zero represents the start of the incubation of pHrodo-beads with cells. DIC, differential interference contrast.

Fig. 3. Time-lapse imaging of the internalization of pHrodo-beads and actin dynamics in HeLa cells. (A) Representative image showing F-actin and the pHrodo beads. F-actin was stained with HMRef. HeLa cells incubated with pHrodo-beads for 52.5 min. Scale bar, 20 μm. (B) Time-lapse images (16.5 – 52.5 min) of the enlarged area encircled by a yellow box in (A) are shown. Scale bar, 10 μm. Arrowheads indicate the early stage of internalization of pHrodo-beads; an arrow indicates maturation or acidification of endosomes containing a pHrodo-bead. Green and magenta colors represent the signals for HMRef (F-actin) and pHrodo-beads, respectively. The time point zero represents the start of the incubation of pHrodo-beads with cells. DIC, differential interference contrast.

Fig. 4. Time-lapse imaging of the internalization of pHrodo-beads into HeLa cells in the presence of TMR-dex10. Time-lapse images (14 – 82 min) are shown. Green and magenta colors represent the signals for pHrodo-beads and TMR-dex10, respectively.

Scale bar, 10 μm. An Arrowhead (at 26 min) indicates the early stage of internalization of pHrodo-beads; arrows indicate maturation or acidification of endosomes containing pHrodo-beads. The time point zero represents the start of the incubation of pHrodo-beads with cells. DIC, differential interference contrast.

Fig. 5. Scanning electron microscopy observation of HeLa cells incubated with pHrodo-beads, with or without treatment of MβCD treatment. (A) Representative images of HeLa cells without (left, control) or with MβCD treatment (right). Magenta arrows indicate representative membrane protrusions under the control condition. Blue arrows indicate representative shorter membrane protrusions on cholesterol depleted condition using MβCD. (B, C) The representative images of HeLa cells incubated with pHrodo-beads without (left, control) or with MβCD treatment (right). White arrows indicate the pHrodo-beads internalized into the cell. (C) The enlarged images of the area encircled by a white box in (B). White arrowheads indicate the representative pHrodo-beads captured by slender protrusions of the plasma membrane; yellow arrowheads indicate ruffle-like membranes. Scale bars, (A) 20 μm; (B) 30 μm (left), 40 μm (right); and (C) 10 μm.

Fig. 6. Time-lapse imaging of HeLa cells incubated with pHrodo-beads using scanning ion conductance microscopy. (A) Observation of the interaction between slender membrane protrusions and the pHrodo-beads on the plasma membrane of HeLa cells. Representative time-lapse images (3 – 22 min) of a pHrodo-bead (3 μm) captured by membrane protrusions. Scale, 0 – 4.8 μm in height. (B) Time-lapse imaging of the internalization of pHrodo-beads into HeLa cells. White arrows show membrane protrusions capturing the pHrodo-beads. Magenta arrowheads show the upper bead. Yellow arrowheads show the lower bead. Green arrowheads show the completely internalized pHrodo-beads. The experiments were repeated at least three times with similar results. Scale, 0 – 8 μm in height. The numbers on the images represent the time (min:sec). The time point zero represents the finish of bead addition to cell culture medium. Scale bars, 2 μm. Note that different height scales are employed in panels A and B.

References

1. M. Sousa de Almeida, E. Susnik, B. Drasler, P. Taladriz-Blanco, A. Petri-Fink and B. Rothen-Rutishauser, *Chem Soc Rev*, 2021, **50**, 5397-5434.
2. A. Combes and G. Franchineau, *Metabolism*, 2019, **100s**, 153944.
3. G. van Niel, G. D'Angelo and G. Raposo, *Nat Rev Mol Cell Biol*, 2018, **19**, 213-228.
4. S. D. Conner and S. L. Schmid, *Nature*, 2003, **422**, 37-44.
5. J. A. Swanson, *Nat Rev Mol Cell Biol*, 2008, **9**, 639-649.
6. S. Tollis, A. E. Dart, G. Tzircotis and R. G. Endres, *BMC Syst Biol*, 2010, **4**, 149.
7. J. A. Swanson and S. Yoshida, *Philos Trans R Soc Lond B Biol Sci*, 2019, **374**, 20180157.
8. S. Kobayashi, T. Kojidani, H. Osakada, A. Yamamoto, T. Yoshimori, Y. Hiraoka and T. Haraguchi, *Autophagy*, 2010, **6**, 36-45.
9. W. Zauner, N. A. Farrow and A. M. Haines, *J Control Release*, 2001, **71**, 39-51.
10. J. Rejman, V. Oberle, I. S. Zuhorn and D. Hoekstra, *Biochem J*, 2004, **377**, 159-169.
11. G. Griffiths, J. Gruenberg, M. Marsh, J. Wohlmann, A. T. Jones and R. G. Parton, *Adv Drug Deliv Rev*, 2022, **188**, 114403.
12. G. Tanaka, I. Nakase, Y. Fukuda, R. Masuda, S. Oishi, K. Shimura, Y. Kawaguchi, T. Takatani-Nakase, U. Langel, A. Gräslund, K. Okawa, M. Matsuoka, N. Fujii, Y. Hatanaka and S. Futaki, *Chem Biol*, 2012, **19**, 1437-1446.
13. T. Takagi, T. Ueno, K. Ikawa, D. Asanuma, Y. Nomura, S. N. Uno, T. Komatsu, M. Kamiya, K. Hanaoka, C. Okimura, Y. Iwadate, K. Hirose, T. Nagano, K. Sugimura and Y. Urano, *Sci Adv*, 2021, **7**, eabg8585.
14. H. Ida, Y. Takahashi, A. Kumatani, H. Shiku, T. Murayama, H. Hirose, S. Futaki and T. Matsue, *Anal Chem*, 2021, **93**, 5383-5393.
15. H. Ida, Y. Takahashi, A. Kumatani, H. Shiku and T. Matsue, *Anal Chem*, 2017, **89**, 6015-6020.
16. M. Miksa, H. Komura, R. Wu, K. G. Shah and P. Wang, *J Immunol Methods*, 2009, **342**, 71-77.
17. G. Maulucci, M. Chiarpotto, M. Papi, D. Samengo, G. Pani and M. De Spirito, *Autophagy*, 2015, **11**, 1905-1916.
18. J. R. Casey, S. Grinstein and J. Orlowski, *Nat Rev Mol Cell Biol*, 2010, **11**, 50-61.
19. R. G. Parton and K. Simons, *Nat Rev Mol Cell Biol*, 2007, **8**, 185-194.

20. J. J. Rennick, A. P. R. Johnston and R. G. Parton, *Nat Nanotechnol*, 2021, **16**, 266-276.
21. Y. Chen, S. Wang, X. Lu, H. Zhang, Y. Fu and Y. Luo, *Blood*, 2011, **117**, 6392-6403.
22. T. Yeung, B. Ozdamar, P. Paroutis and S. Grinstein, *Curr Opin Cell Biol*, 2006, **18**, 429-437.
23. T. A. Masters, B. Pontes, V. Viasnoff, Y. Li and N. C. Gauthier, *Proc Natl Acad Sci U S A*, 2013, **110**, 11875-11880.
24. J. Loh, M. C. Chuang, S. S. Lin, J. Joseph, Y. A. Su, T. L. Hsieh, Y. C. Chang, A. P. Liu and Y. W. Liu, *J Cell Sci*, 2019, **132**.
25. D. C. Barral, M. Cavallari, P. J. McCormick, S. Garg, A. I. Magee, J. S. Bonifacino, G. De Libero and M. B. Brenner, *Traffic*, 2008, **9**, 1446-1457.
26. C. D. Williamson and J. G. Donaldson, *Mol Biol Cell*, 2019, **30**, 1477-1489.
27. V. Jaumouille, A. X. Cartagena-Rivera and C. M. Waterman, *Nat Cell Biol*, 2019, **21**, 1357-1369.
28. M. Kuriyama, H. Hirose, T. Masuda, M. Shudou, J. V. V. Arafiles, M. Imanishi, M. Maekawa, Y. Hara and S. Futaki, *Sci Rep*, 2022, **12**, 6322.
29. M. C. Kerr and R. D. Teasdale, *Traffic*, 2009, **10**, 364-371.
30. C. Commisso, R. J. Flinn and D. Bar-Sagi, *Nat Protoc*, 2014, **9**, 182-192.

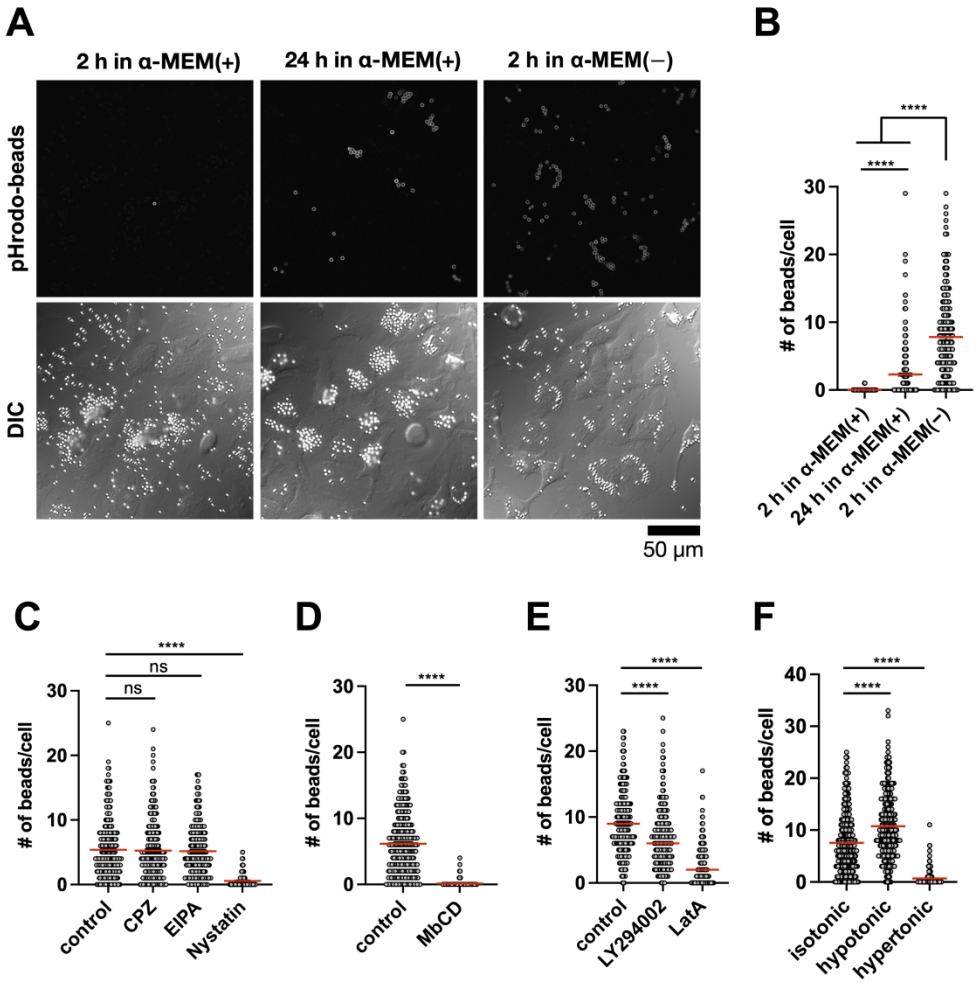

Fig.1. Observation and quantification of pHrodo-beads (3 μm) internalized into HeLa cells.

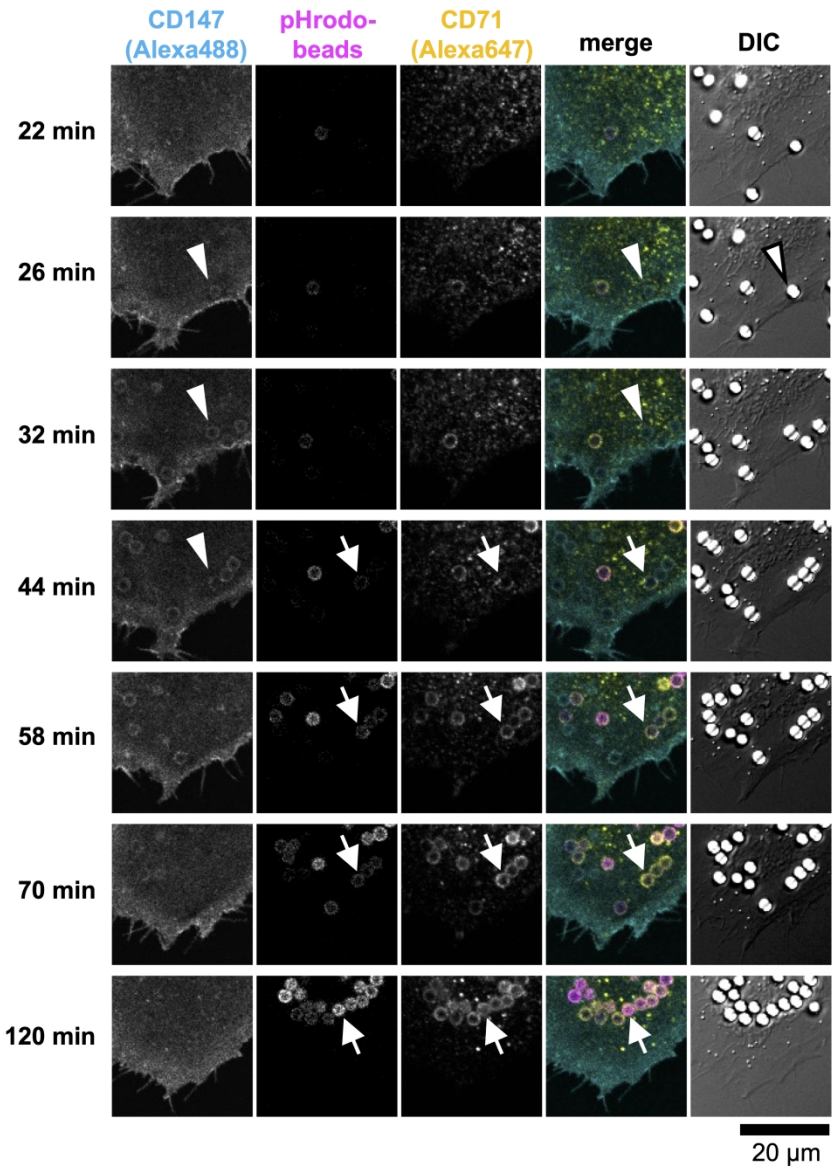

Fig. 2. Time-lapse imaging of the internalization of pHrodo-beads into HeLa cells stained with Alexa-labeled antibodies against CD147 and CD71.

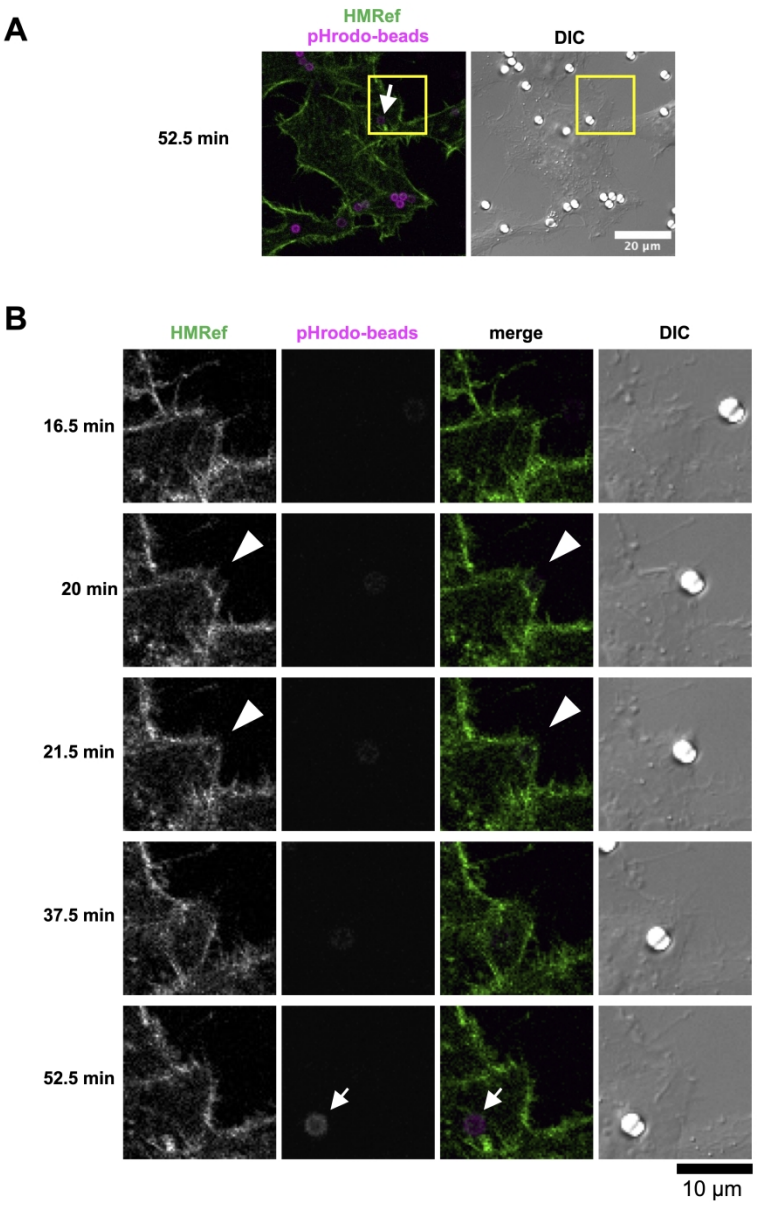

Fig. 3. Time-lapse imaging of the internalization of pHrodo-beads and actin dynamics in HeLa cells.

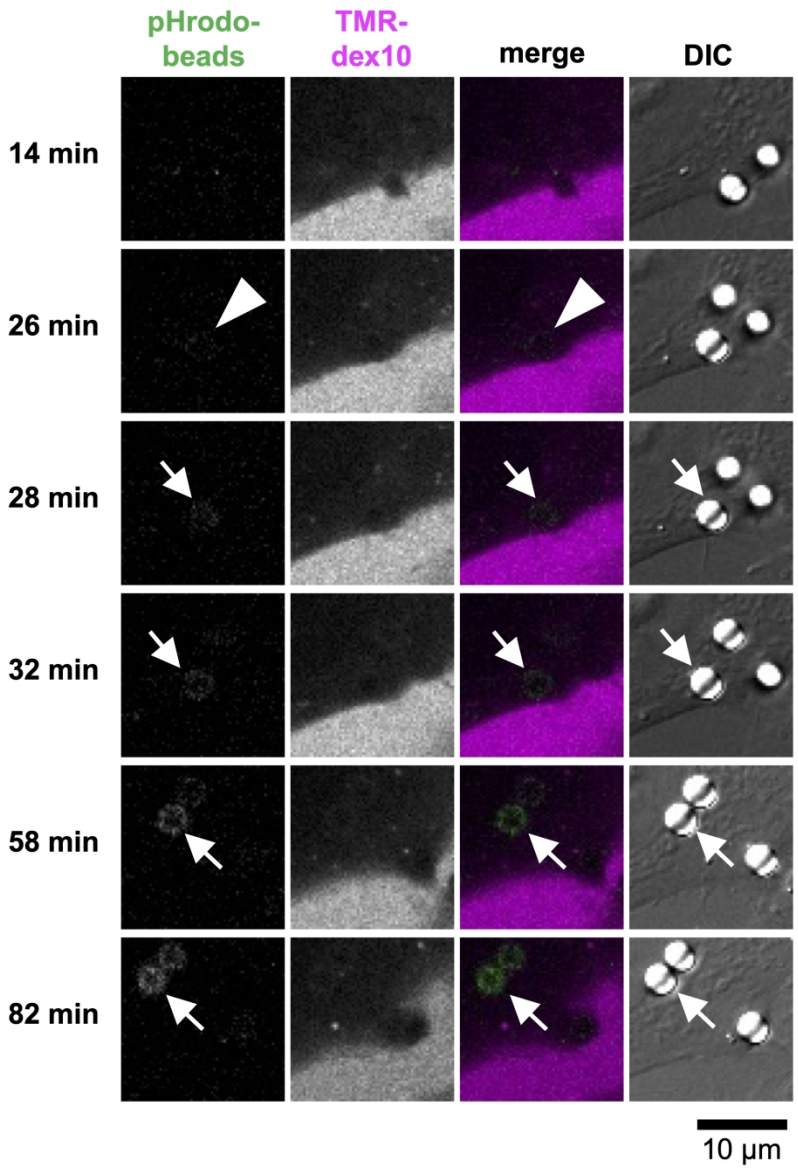

Fig. 4. Time-lapse imaging of the internalization of pHrodo-beads into HeLa cells in the presence of TMR-dex10.

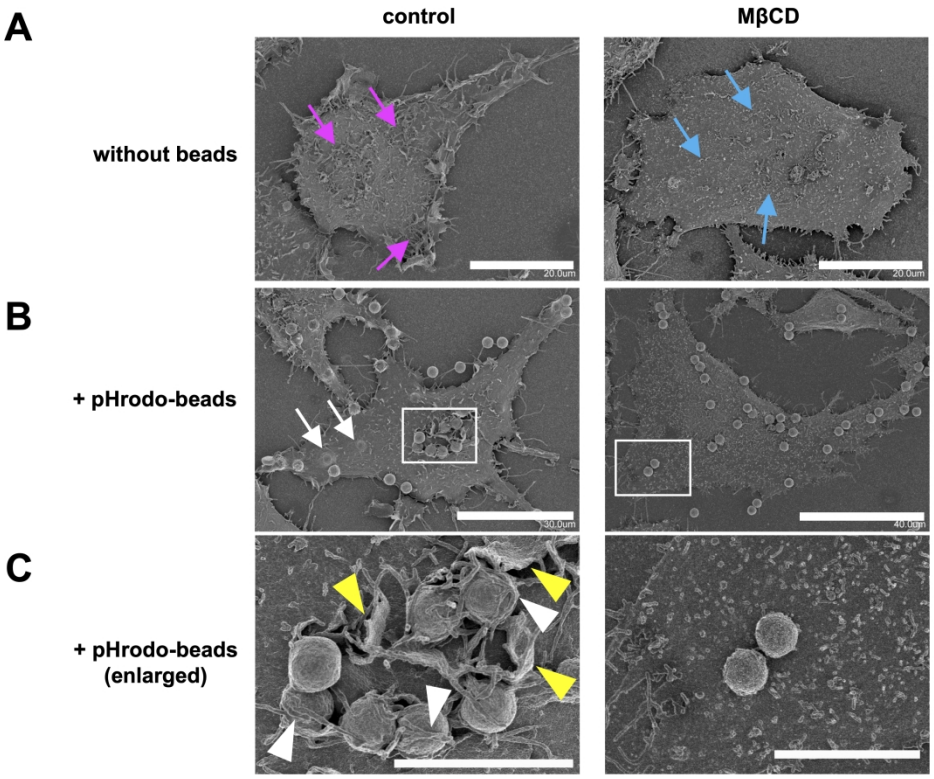

Fig. 5. Scanning electron microscopy observation of HeLa cells incubated with pHrodo-beads, with or without treatment of MβCD treatment.

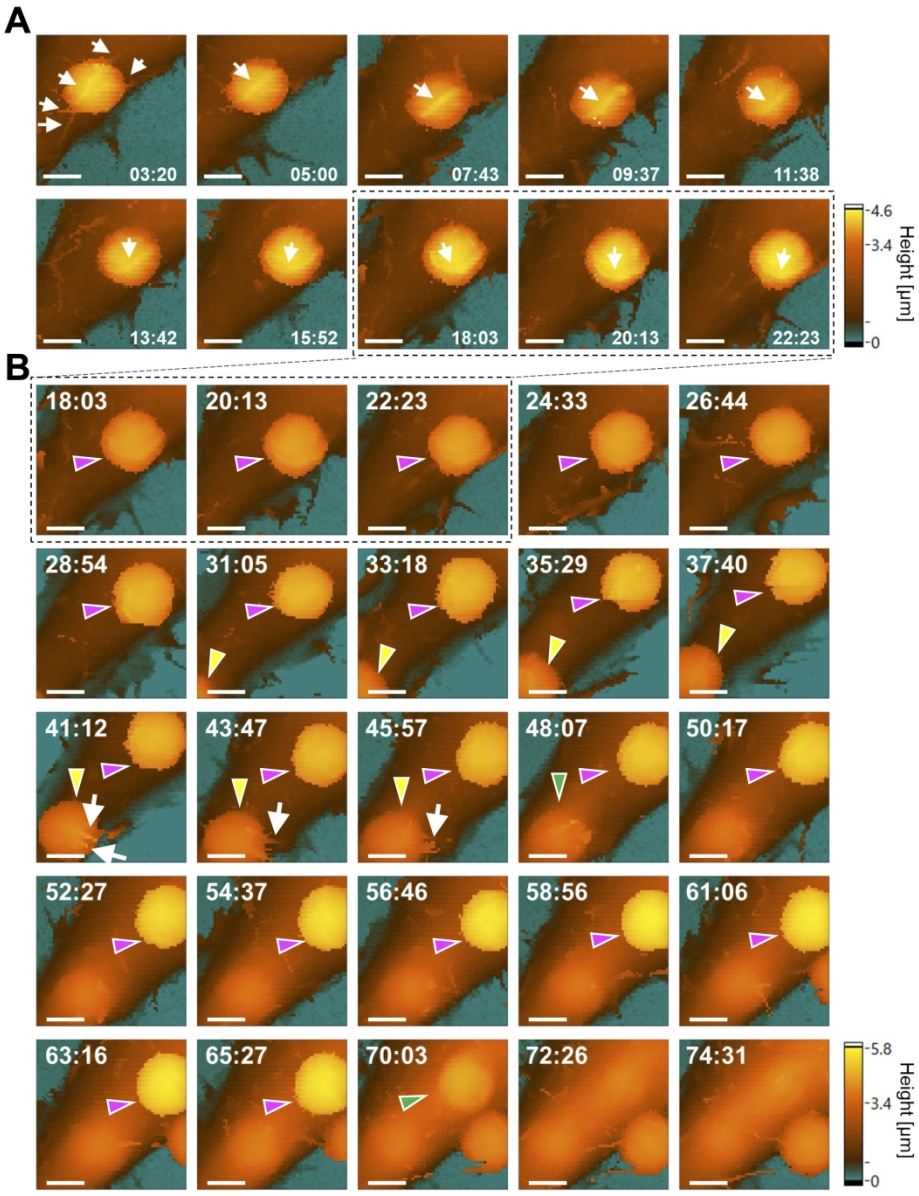

Fig. 6. Time-lapse imaging of HeLa cells incubated with pHrodo-beads using scanning ion conductance microscopy.